scientific reports

Check for updates

OPEN

Significantly enhancement of sunlight photocatalytic performance of ZnO by doping with transition metal oxides

Alfonso E. Ramírez[1]✉, Marly Montero-Muñoz[2], Lizbeth L. López[3], J. E. Ramos-Ibarra[2], Jose A. H. Coaquira[2], Benoît Heinrichs[4] & Carlos A. Páez[4]

In this study we report, the synthesis of ZnO and its doping with Transition Metal Oxides -TMO-, such as Cr_2O_3, MnO_2, FeO, CoO, NiO, Cu_2O and CuO. Various characterization techniques were employed to investigate the structural properties. The X-ray diffraction (XRD) data and Rietveld refinement confirmed the presence of TMO phases and that the ZnO structure was not affected by the doping with TMO which was corroborated using transmission Electron microscopy (TEM). Surface areas were low due to blockage of adsorption sites by particle aggregation. TMO doping concentration in the range of 3.7–5.1% was important to calculate the catalytic activity. The UV–Visible spectra showed the variation in the band gap of TMO/ZnO ranging from 3.45 to 2.46 eV. The surface catalyzed decomposition of H_2O_2 was used as the model reaction to examine the photocatalytic activity following the oxygen production and the systems were compared to bulk ZnO and commercial TiO_2-degussa (Aeroxyde-P25). The results indicate that the introduction of TMO species increase significantly the photocatalytic activity. The sunlight photocatalytic performance in ZnO-doped was greater than bulk-ZnO and in the case of MnO_2, CoO, Cu_2O and CuO surpasses TiO_2 (P25-Degussa). This report opens up a new pathway to the design of high-performance materials used in photocatalytic degradation under visible light irradiation.

The importance of raising global awareness about how light-based technologies promote sustainable development and provide solutions to global challenges has recognized by the United Nations[1] In the environmental field, light can play a vital role, because its combination with semiconductor materials it provides a great power for photodegradation[2]. It is well known the use of semiconductors like TiO_2[3] and ZnO for this purpose[4]. Likewise, it is known that the wide band gap of these metal oxides limits their use in the visible range[5]. Additionally, rapid recombination of hole-electrons pairs is another limitation of ZnO[6].

Therefore, the development of new generation nanophotocatalysts is a challenge for improving their photocatalytic activity in visible light. In the case of ZnO its application has been limited due to its large band gap[7], which can decrease the photocatalytic properties[8]. One strategy to enhance their performance and its use with a light source, is doping with different elements and/or its compounds[9]. In case of ZnO, doping with the noble metals where Ag is most reported[10–13], but we can find reports for Pd[14], Pt[15] and Au[16,17]. Other elements that have received special attention correspond to the lanthanide series[18] specifically Ce[19,20], Eu[21], Gd[22,23] and La[24]. Others metals of *d*-type that are also studied include Fe[25], Ni[26,27], Mn[28,29], Co[30,31] and Cu[32–34].

The surface catalyzed decomposition of H_2O_2 has been reported as useful, simple and inexpensive way to evaluate the catalytic activity on solids under UV–visible light irradiation[35–37]. In this work, we have used the surface photodecomposition of H_2O_2 to show that doping ZnO with transition metal oxides -TMO-, enhance the photocatalytic powder of ZnO. In the case of doping with MnO_2, Co_2O_3 and CuO, the resulting systems can become possible substitutes to most efficient commercial photocatalyst: Aeroxide TiO_2/P25. This new information can be utilized to the future design of materials for the photocatalytic degradation under visible light irradiation.

[1]Grupo de Catalisis, Departmento de Química, Universidad del Cauca, Popayán - Cauca, Colombia. [2]Institute of Physics, University of Brasilia, Brasília, DF 70910-900, Brazil. [3]Grupo de Investigación en Electroquímica Y Medio Ambiente, Facultad de Ciencias Básicas, Universidad Santiago de Cali, Cali, Colombia. [4]Department of Chemical Engineering, Génie chimique—Nanomatériaux et Interfaces, Université de Liège, Liege, Belgium. *†Carlos A. Paez—Deceased. ✉email: aramirez@unicauca.edu.co

Results and discussion

Characterization. Zinc oxide phase corresponding to the wurtzite hexagonal structure (PDF 00–900-4179), with space group P63mc is the main phase as can be seen in Fig. 1. In addition to the ZnO main phase, reflections related to transition metal oxide dopant phase (see in the insets of Fig. 1) are determined. The following TMO phases were identified CuO (PDF 00–901-6057), Cu_2O (PDF 00–900-7497), CoO (PDF 00–591-0031), Cr_2O_3 (PDF 00–900-7442), Fe_2O_3 (PDF 00–901-6457), NiO (PDF 00.432–0493) and MnO_2 (PDF 00–151-4237).

In order to determine additional information, the XRD patterns were analyzed using the Rietveld refinement method. It was determined that the doping with TMO did not affect the wurtzite structure of ZnO, since all characteristic reflections of ZnO phase were also obtained in the XRD pattern of TMO/ZnO samples[38]. The lattice constants, unit cell volume and percentage of phases are listed in Table 1. In all of cases, the static structure factor of the wurtzite phase ($c/a \sim 1.602$) remains constant. It suggests that essentially no changes were determined in the lattice constants of the wurtzite phase, implying that the transition metal did not diffuse into the ZnO structure, in agreement with that reported in the literature[39]. Otherwise, the diffusion could lead to the substitution of Zn ions by the transition metal ions and it could lead to changes in the lattice constants of the wurtzite structure, which is not observed.

TEM measurements were performed in order to get more information about the crystalline structure of the photocatalysts, mainly the particle size. Figure 2 shows the typical TEM images of the synthesized catalysts. Figure 2a shows the ZnO nanoparticles with a hexagonal structure and Fig. 2b presents ZnO powder modified with TMO.

As shown in Fig. 2a we can inferred the mean size of the ZnO nanoparticles, which is close to 47 ± 5 nm. In Fig. 2b is shown that the particles are in the nanoscale (approximately 50–60 nm in size) and reveals: (i) an increase in size, may be as a result of the TMO surface covering of ZnO nanoparticles[40] and (ii) the conservation of hexagonal structure, indicating that the structure of ZnO is not notoriously affected by the TMO doping, in agreement with XRD data analysis.

The BET surface areas of our samples were determined and the values are listed in Table 2. ZnO exhibits a low surface area that reveal the effect of calcination as reported in the literature[41]. It is determined that the TMO-doped ZnO samples show smaller surface area in comparison to the surface area of pure ZnO. That surface area change was attributed to the particles aggregation and; thus, to the partial blockage of adsorption sites[42].

The optical characterization of materials allows the prediction of possible behavior of photocatalysts under illumination. Absorbance spectra, Fig. 3a, have been used to determine the optical band *gap* energy (E_g). The values of E_g (Table 2) were determined using the Tauc's plot method, Fig. 3b.

In all of cases, the band *gap* of TMO-doped ZnO are smaller in comparison to pure ZnO, being the smallest for the CoO/ZnO sample (2.46 eV). These results are in agreement with other works such as NiO/ZnO nanorods[43] and CoO/ZnO nanofibers[44]. As a consequence of the coupling of MTO and ZnO in the heterojunction more electrons are freely transferred from M^{n+} of the TMO (with higher Fermi level) to ZnO (with lower level), promoting the separation of holes and electrons and, then, effective heterojunctions are formed[43]. Therefore, the band gap closing can facilitate stepping electrons from the valence band to the conduction band as that reported in the literature for CuO-ZnO nanocomposites[45]. That band gap closing leads to the photocatalytic activity improvement of the TMO-doped ZnO nanocomposites.

Photocatalytic H_2O_2 decomposition. *Control test.* The reaction in the dark condition as a function of time was followed. This control test confirmed that H_2O_2 is not decomposed in the dark condition. In the absence of catalyst but under visible light irradiation, 0.65×10^{-4} mol of O_2 were produced and this control test allows us affirm that decomposition rates are related only to the effect of light on the TMO/ZnO systems (Fig. 4).

Photocatalytic systems. To understand the behavior of the materials in the reaction, we follow the O_2 formation as a function of time under visible light irradiation.

The Table 3 shows the production of O_2 form the decomposition of H_2O_2 during 20 min. As observed, there is a progressive increase in the O_2 production. The conducting properties of the catalysts enhance the production of O_2 and therefore the H_2O_2 decomposition.

The Fig. 5 shows the kinetic study of the photocatalytic decomposition of H_2O_2 carried out using the TMO-ZnO systems. As observed, the O_2 production obeys the first-order law, as previously reported in the literature[46]. The inset shows the initial rate (the slopes of the plots correspond to the rate constants). These rate constants are different and indicate distinct response of the systems, Table 4.

The irradiation without catalysts just promotes a weak H_2O_2 decomposition and leads to the O_2 production 0.65×10^{-4} mol, while the use of ZnO increases the O_2 production up to 1.5 times (Table 3) demonstrating the catalytic power of ZnO. Nevertheless, the doping of ZnO with MTO significantly enhance the photocatalytic power of ZnO, which suggests that the surface charge transfer process should increase, meanwhile, the electron—hole recombination rate should decrease[42]. In fact, the O_2 production (Table 3) can go up to 3.95×10^{-4} mol in the presence of CoO/ZnO, which seems to be the system with the highest activity. Additionally, it was determined that the Aeroxide TiO_2-P25 power can be exceed by the ZnO doping with transition metal oxides, specially Cu_2O, CuO, MnO_2 and CoO.

Table 4 shows the reaction rate and the catalytic activity values. These parameters corroborate that the best dopant oxides are those previously mentioned. These results have been correlated with the redox potential and the amount of loaded metal ion[47]. Mn^{+4}, Cu^{+2}, Co^{+2}, Cu^{+1} and Fe^{+3} have positive values and the low rate observed with Cr^{+3} and Ni^{+2} is in agreement with their negative redox potentials[48].

The introduction of TMO in ZnO improves its absorption in the visible region, Fig. 3a This leads to reduce the extent of undesired recombination of charge carrier resulting in a better activity[49] and a decrease of the

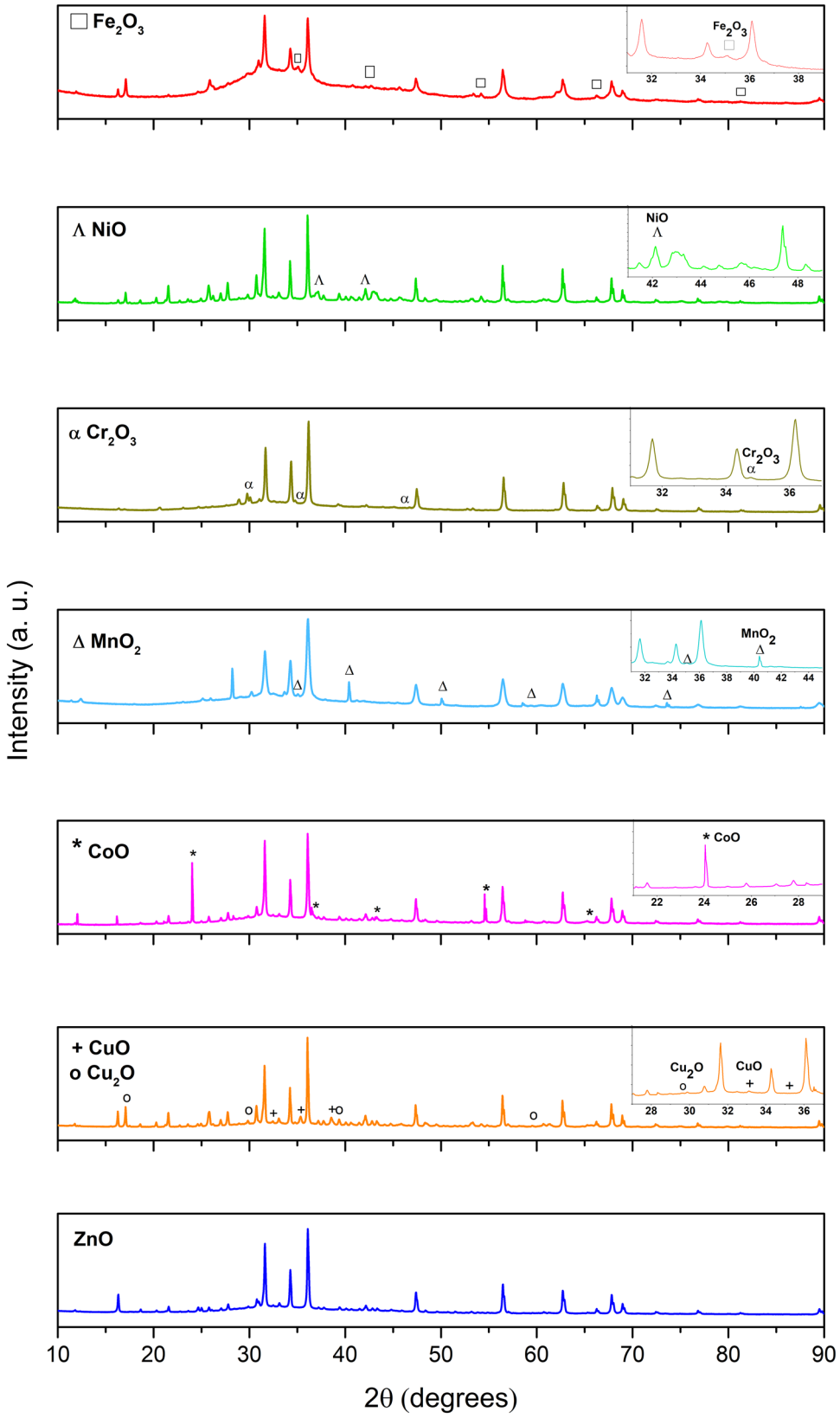

Figure 1. XRD patterns of transition metal oxides-doped ZnO nanoparticles. In the insets are shown reflections corresponding to the TMO dopant phase.

Catalyst	Wurtzite phase					TMO phase		
	a (Å)	c (Å)	c/a	V (Å^3)	%	a (Å)	c (Å)	%
ZnO	3.2484	5.2046	1.602	47.56	100	–	–	0
CoO/ZnO	3.2498	5.2052	1.602	47.61	96	5.1842	3.0172	4
Cu_2O–CuO/ZnO	3.2497	5.2060	1.602	47.61	76	4.6539	5.1083	16
						4.2521	4.2521	8
MnO_2/ZnO	3.2514	5.2107	1.603	47.71	79	4.3886	2.8653	21
Cr_2O_3/ZnO	3.2485	5.2048	1.602	47.57	94	5.3524	5.3524	6
NiO/ZnO	3.2483	5.2037	1.602	47.55	89	4.1684	4.1684	11
Fe_2O_3/ZnO	3.2477	5.2028	1.602	47.59	82	5.4375	5.4375	18

Table 1. Lattice parameters and percentage of phases obtained from the Rietveld refinement of the XRD patterns.

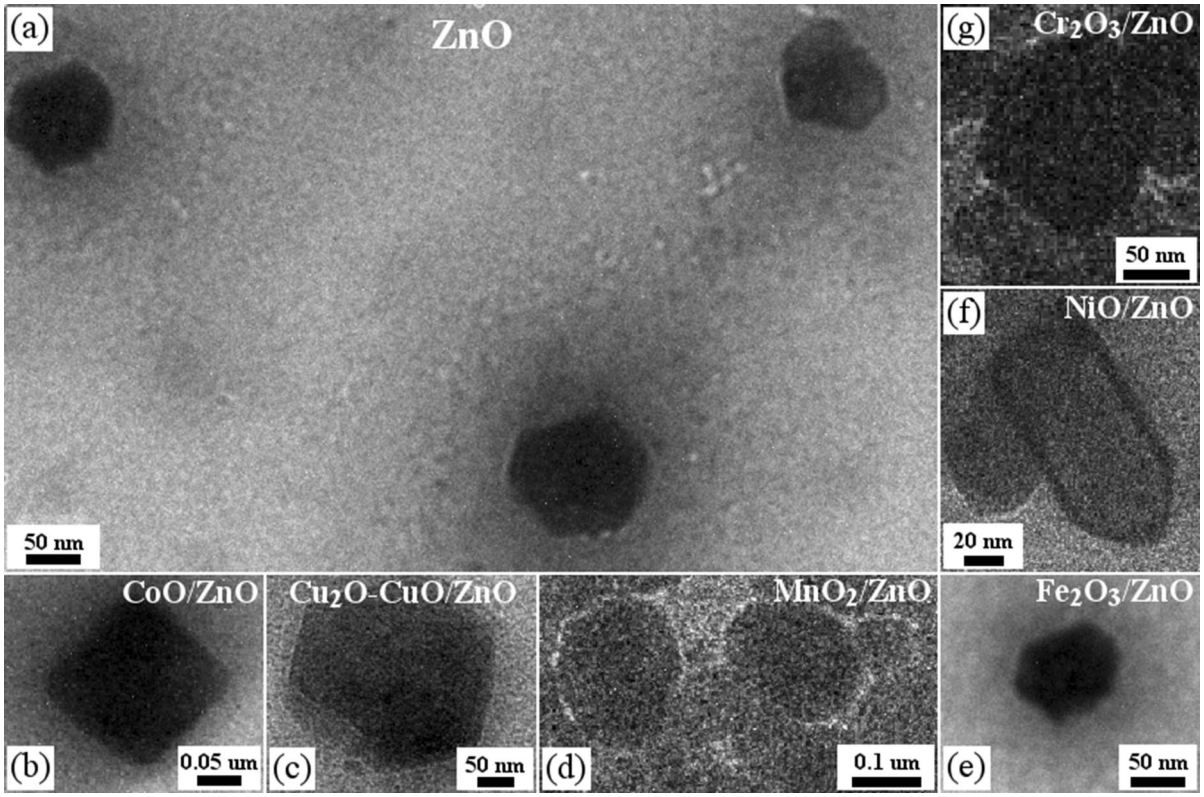

Figure 2. (**a**) ZnO nanoparticles obtained. (**b**) TMO-doped ZnO. (**c**) Cu_2O-CuO-doped ZnO. (**d**) MnO_2-doped ZnO. (**e**) Fe_2O_3-doped ZnO

Catalyst	%[a] (w/w) M	S_{BET} (m^2/g)	Band gap energy (eV)
ZnO	–	8.5	3.20
CoO/ZnO	4.3	2.5	2.46
Cu_2O–CuO/ZnO	5.2	1.3	3.12
MnO_2/ZnO	4.9	3.9	2.98
Cr_2O_3/ZnO	3.7	1.9	3.02
NiO/ZnO	5.0	2.5	3.15
Fe_2O_3/ZnO	5.1	4.8	2.92

Table 2. Main characteristics of catalysts used in the H_2O_2 photodecomposition. [a]% (w/w) M represents the dopant content.

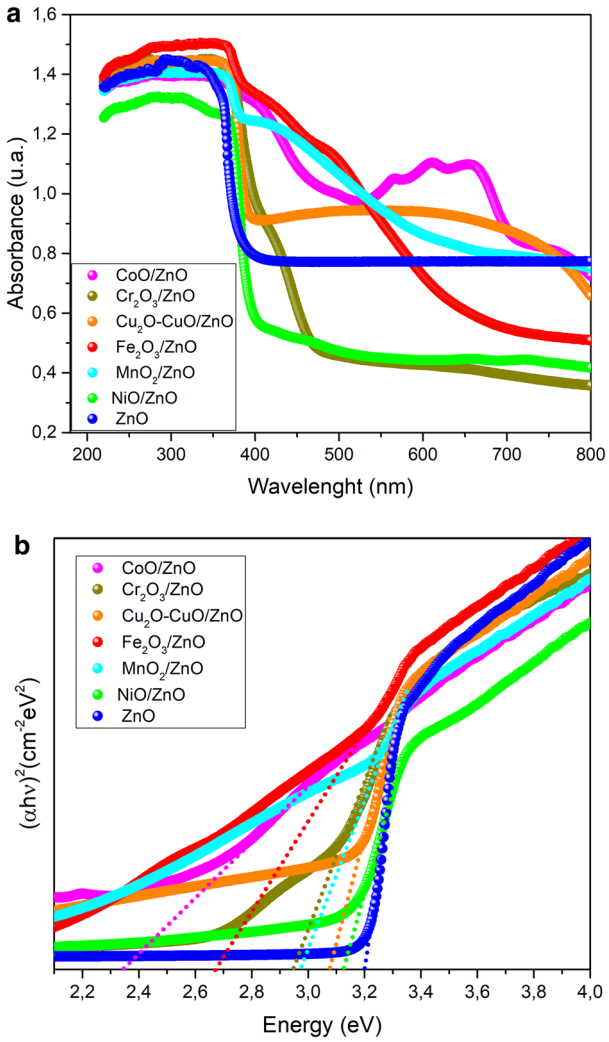

Figure 3. (**a**) UV–Vis spectra for photocatalysts. (**b**) Tauc´s plot for band *gap* determination of TMO-doped ZnO.

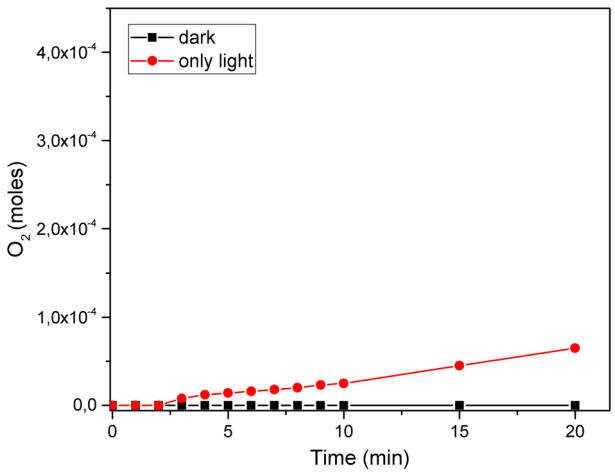

Figure 4. Control tests for the decomposition of H_2O_2.

Catalysts	O_2 production[a] ($mol \times 10^{-4}$)
None	0.65
ZnO	1.00
CoO/ZnO	3.95
Cu_2O–CuO/ZnO	3.99
MnO_2/ZnO	3.66
Cr_2O_3/ZnO	2.16
NiO/ZnO	1.87
Fe_2O_3/ZnO	2.12
Aeroxide TiO_2/P25	3.45

Table 3. Production of O_2 by H_2O_2 decomposition in presence of photocatalytic systems. [a]During 20 min.

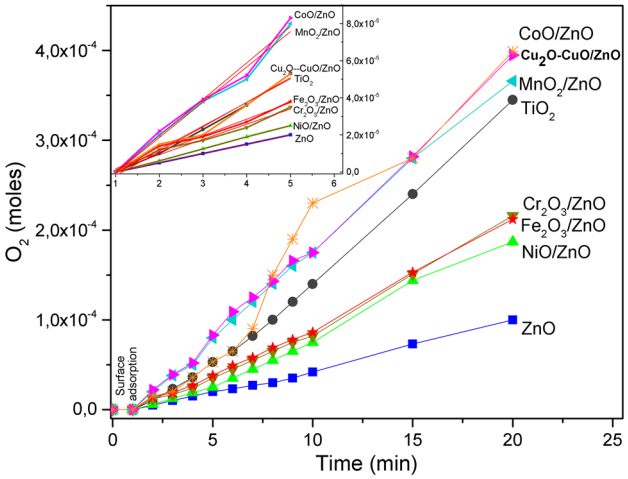

Figure 5. Kinetic study of the H_2O_2 decomposition carried out using the MTO-ZnO systems under light visible irradiation.

Catalysts	Rate constant ($min^{-1} \times 10^{-5}$)	Catalytic activity (O_2 moles min^{-1} M^{n+} $moles^{-1}$)
CoO/ZnO	1.96	5.4
Cu_2O–CuO/ZnO	1.27	3.1
MnO_2/ZnO	1.90	4.2
Cr_2O_3/ZnO	0.82	2.3
NiO/ZnO	0.63	1.5
Fe_2O_3/ZnO	0.89	1.9

Table 4. Rate constants and catalytic activities for photocatalytic systems.

value of band gap, which leads to higher efficiency of photocatalysts due to a better overlap with the light source spectrum[50].

The H_2O_2 decomposition under visible light irradiation by different semiconductors SC as TiO_2[51] or MnO_2[35] has been studied and the mechanism is based on the oxidation–reduction properties of SC. For ZnO can be understood as follows: the irradiation of ZnO leads to excited state that can be expressed as ZnO (e^-, h^+) (reaction R.1). The electron in the conduction band -CB- is available for transference (reaction R.2) while photoinduced valence band holes is open for donation (reaction R.3).

$$\mathrm{ZnO} \xrightarrow{h\nu} \mathrm{ZnO}\left(\mathrm{e}^-, \mathrm{h}^+\right) \tag{R.1}$$

$$\mathrm{h}^+ + \mathrm{H_2O_2} \rightarrow \mathrm{H}^+ + \mathrm{HO_2^{\cdot}} \tag{R.2}$$

$$\mathrm{e}^- + \mathrm{H_2O_2} \rightarrow \mathrm{HO}^{\cdot} + \mathrm{OH}^- \tag{R.3}$$

$$H_2O_2 \rightarrow 1/2O_2 + H_2O \quad (R.4)$$

A direct interfacial charge transfer mechanism is proposed for the visible light activity in M^{n+}-modified samples[52]. Firstly, the adsorption of H_2O_2 by the TMO/ZnO system releases H^+ ions (reaction R.5). The electrons transferred to the CB of TMO from the valence band -VB- of ZnO lead to the metal reduction (reaction R.6). The catalyst regeneration step involves the $HO^{\cdot}$ reduction to HO^- (reaction R.8).

$$M^{n+}/ZnO + H_2O_2 \rightarrow M^{n+}/ZnO\,(HO_2)^- + H^+ \quad (R.5)$$

$$M^{n+}/ZnO\,(HO_2)^- + H^+ \xrightarrow{hv} M^{(n-1)+}/ZnO + HO_2^{\cdot} \quad (R.6)$$

$$HO_2^{\cdot} + H_2O_2 \rightarrow HO^{\cdot} + O_2 + H_2O \quad (R.7)$$

$$M^{(n-1)+}/ZnO + HO^{\cdot} \rightarrow M^{n+}/ZnO + HO^- \quad (R.8)$$

Therefore, in the two pathways, the free radicals $HO_2^{\cdot}$ (R.2 and R.6) or $HO^{\cdot}$ (R.3) induce the chain reactions sequence to produce the final products, H_2O and O_2 (reaction R.4 and R.7).

Methods

Preparation of ZnO and MTO-doped ZnO. ZnO and MTO-doped ZnO were prepared by the sol–gel method using a precursor alkaline solution composed of zinc acetate dihydrate dissolved in methanol, as described in a literature[53]. In all cases, the dopant source of MT was nitrate except in the case of Mn, which was chloride. In a representative preparation, ZnO and MTO-doped ZnO were synthesized by the slow hydrolysis of zinc acetate using KOH as precursor. Zinc acetate dehydrate and a dopant were first dissolved in methanol and mixed together with a KOH solution (0.4 M) for obtain a clear and homogeneous solution. The solution was stirred at 60 °C for 2 h. Finally, the gel washed, dried and powdered before calcinations at 450 °C for eight hours in a muffle furnace. In Table 2 is shown the doped metal content determined from XRF measurements.

Characterization of ZnO and MTO-doped ZnO. X-ray diffraction analysis was performed using a RIGAKU Ultima IV diffractometer, with a Cu-K_α as radiation source and Ni-filtered with CBO monochromator. Operating voltage was 45 kV with beam current of 15 mA. The measurements were performed at step widths of 0.05 and the scan rate was maintained at 2° min^{-1}. The XRD of the samples were performed in the 2θ range of 20–70° as in[54]. Additionally, the XRD data were analyzed using the Rietveld refinement method via the FullProf program. QUALX2.0 software was used for phase identification in the qualitative analysis from powder diffraction data.

Transmission electron microscopy (TEM) images were obtained by using a microscope (JOEL, model 1011) to determine the morphology, the mean particles size and the size distribution as in[54].

The content of metal was estimated by Energy Dispersive X-ray technique using a EDX-720 Shimadzu Fluorescence Spectrometer (XRF). The solids were prepared as loose powder. The analysis was made using a Rh X-ray tube for 200 s under vacuum.

The UV–Vis spectra of samples were recorded in the range of 220–1000 nm using UV-2600 Shimadzu spectrophotometer.

For nitrogen adsorption–desorption, the measures were made at − 196 °C with a Fisons Sorptomatic 1990, after outgassing at 10^{-3} Pa for 24 h at ambient temperature.

Photocatalytic degradation of H_2O_2. Degradation of H_2O_2 under visible light simulated conditions, with an halogen lamp (300 W, 220 V, λ ≥ 400 nm), was used to evaluate the photocatalytic activity of ZnO and MTO-doped ZnO following the report made by Paéz et al.[35]. The initial pH was kept between 4.6–5.1. 5 mg of solid was suspended in 50 mL of deionized water in the reactor and ultra-sounded for 30 min; when the temperature was 20 °C, 10 mL of H_2O_2 solution were injected into the solid suspension and the lamp was turned on under visible light radiation. The production (in mol) of oxygen was calculated by the change in H_2O_2 concentration during photocatalytic run and has been determined from Eq. (1).

$$C = Co - 2 \times \frac{PV_g}{RTV_L} \quad (1)$$

where C is the concentration of H_2O_2 at time t (mol L^{-1}), C_0 the initial concentration of H_2O_2 (6.5 mol L^{-1}), P the atmospheric pressure (≅ 101.3 kPa), R is the gas constant (8.314 L kPa mol^{-1} K^{-1}), V_L the total volume of solution (0.015 L), T is the room temperature and V_g corresponds to the integrated volume of gas liberated until time t (L) at atmospheric pressure measured by the devices.

Conclusion

TMO/ZnO nanocomposites were successfully synthesized and tested their photocatalytic activity for H_2O_2. The morphological and structural results confirmed that the TMO doping did not provoke the ions substitution in the ZnO lattices and that the ZnO structure is not affected. Optical measurements showed the ZnO band gap decrease with the doping. It is found that the doping reduces the electron–hole recombination rate, which improves the absorption in the visible region and leads to a significantly enhancement of sunlight photocatalytic

performance of ZnO. The surface-mediated decomposition of H_2O_2 and the consequent production of O_2 were used to measure the photocatalytic power of the TMO/ZnO nanocomposites. The resultant reaction rate values are explained based on the combination of redox potential of metal of the TMO and a better absorption of visible light due to the presence of TMO in the TMO/ZnO system. Our findings indicate that Cu_2O/ZnO, CuO/ZnO, MnO_2/ZnO and CoO/ZnO systems overcomes the photocatalytic activity of most popular commercial photocatalyst: Aeroxide P25. Therefore, our results indicate that TMO/ZnO systems can substitute the current commercial photocatalysts.

Received: 29 April 2020; Accepted: 17 November 2020
Published online: 02 February 2021

References

1. United Nations Educational, Scientific and Cultural Organization. 37C/Resolution 15. https://unesdoc.unesco.org/ark:/48223/pf0000226162 (2013).
2. Hoffman, M. R., Martin, S. T., Choi, W. & Bahnemann, D. W. Environmental applications of semiconductor photocatalysis. *Chem. Rev.* **95**(1), 69–96 (1995).
3. Chen, X. & Mao, S. S. Titanium dioxide nanomaterials: synthesis, properties, modifications, and applications. *Chem. Rev.* **107**(7), 2891–2959 (2007).
4. Ali, A. M. *et al.* Doped metal oxide (ZnO) and photocatalysis: a review. *J. Pak. Inst. Chem. Eng.* **40**(1), 11–19 (2012).
5. Ebrahimi, R. *et al.* Effects of doping zinc oxide nanoparticles with transition metals (Ag, Cu, Mn) on photocatalytic degradation of Direct Blue 15 dye under UV and visible light irradiation. *J. Environ. Health Sci. Eng.* **17**(1), 479–492 (2019).
6. Xu, C. *et al.* Preparation, characterization and photocatalytic activity of Co-doped ZnO powders. *J. Alloys Compd.* **497**(1–2), 373–376 (2010).
7. Vijayakumar, G. N. S., Devashankar, S., Rathnakumari, M. & Sureshkumar, P. Synthesis of electrospun ZnO/CuO nanocomposite fibers and their dielectric and nonlinear optic studies. *J. Alloys Compd.* **507**, 225–229 (2010).
8. Dijken, A. V., Janssen, A. H., Smitsmans, M. H. P., Vanmaekelbergh, D. & Meijerink, A. Size-selective photoetching of nanocrystalline semiconductor particles. *Chem. Mater.* **10**, 3513–3522 (1998).
9. Tong, H. *et al.* Nano-photocatalytic materials: possibilities and challenges. *Adv. Mater.* **24**, 229–251 (2012).
10. Liu, Y., Wei, S. & Gao, W. Ag/ZnO heterostructures and their photocatalytic activity under visible light: effect of reducing medium. *J. Hazard. Mater.* **287**, 59–68 (2015).
11. Zheng, Y. *et al.* Photocatalytic activity of Ag/ZnO heterostructure nanocatalyst: correlation between structure and property. *J. Phys. Chem. C* **112**, 10773–10777 (2008).
12. Ren, C., Yang, B., Wu, M., Xu, J., Fu, Z., lv, Y., Guo, T., Zhao, Y. & Zhu, C. Synthesis of Ag/ZnO nanorods array with enhanced photocatalytic performance. *J. Hazard. Mater.* **182**, 123–129 (2010).
13. Yin, X. T., Que, W. X., Liao, Y. L., Zhang, J. & Shen, F. Y. Ag–ZnO composite nanocrystals: synthesis, characterization and photocatalytic properties. *Mater. Res. Innov.* **16**(3), 213–218 (2012).
14. Zhanga, Y., Wanga, Q., Xub, J. & Ma, S. Synthesis of Pd/ZnO nanocomposites with high photocatalytic performance by a solvothermal method. *Appl. Surf. Sci.* **258**, 10104–10109 (2012).
15. Morales-Flores, N., Pal, U. & Sánchez Mora, E. Photocatalytic behavior of ZnO and Pt-incorporated ZnO nanoparticles in phenol degradation. *Appl. Catal. A Gen.* **394** 269–275 (2011).
16. Georgiev, P. *et al.* Effect of gold nanoparticles on the photocatalytic efficiency of ZnO films. *Colloids Surf. A Physicochem. Eng. Asp.* **460**, 240–247 (2014).
17. Silva, C. G. *et al.* Developing highly active photocatalysts: gold-loaded ZnO for solar phenol oxidation. *J. Catal.* **316**, 182–190 (2014).
18. Kaneva, N., Bojinova, A., Papazova, K. & Dimitrov, D. Photocatalytic purification of dye contaminated sea water by lanthanide (La^{3+}, Ce^{3+}, Eu^{3+}) modified ZnO. *Catal. Today* **252**, 113–119 (2015).
19. Lamba, R., Umar, A., Mehta, S. K. & Kansal, S. K. CeO_2/ZnO hexagonal nanodisks: Efficient material for the degradation of direct blue 15 dye and its simulated dye bath effluent under solar light. *J. Alloys Compd* **620**, 67–73 (2015).
20. Chang, C. J., Lin, C. Y. & Hsu, M. H. Enhanced photocatalytic activity of Ce-doped ZnO nanorods under UV and visible light. *J. Taiwan Inst. Chem. Eng.* **45**(4), 1954–1963 (2014).
21. Zong, Y., Li, Z., Wang, X., Ma, J. & Men, Y. Synthesis and high photocatalytic activity of Eu-doped ZnO nanoparticles. *Ceram. Int.* **40**, 10375–10382 (2014).
22. Luo, Y. *et al.* Fabrication and photocatalytic properties of Gd-doped ZnO nanoparticle-assembled nanorods. *Mater. Lett.* **149**, 70–73 (2015).
23. Kumar, S. & Sahare, P. D. Gd^{3+} incorporated ZnO nanoparticles: a versatile material. *Mater. Res. Bull.* **51**, 217–223 (2014).
24. Raza, W., Haque, M. M. & Muneer, M. Synthesis of visible light driven ZnO: Characterization and photocatalytic performance. *Appl. Surf. Sci.* **322**, 215–224 (2014).
25. Xie, J. *et al.* Synthesis of α-Fe_2O_3/ZnO composites for photocatalytic degradation of pentachlorophenol under UV–Vis light irradiation. *Ceram. Int.* **41**, 2622–2625 (2015).
26. Kaneva, N. V., Dimitrov, D. T. & Dushkin, C. D. Effect of nickel doping on the photocatalytic activity of ZnO thin films under UV and visible light. *Appl. Surf. Sci.* **257**, 8113–8120 (2011).
27. Ekambaram, S., Iikubo, Y. & Kudo, A. Combustion synthesis and photocatalytic properties of transition metal-incorporated ZnO. *J. Alloys Compd.* **433**(1–2), 237–240 (2007).
28. Mahmood, M. A., Baruah, S. & Dutta, J. Enhanced visible light photocatalysis by manganese doping or rapid crystallization with ZnO nanoparticles. *Mater. Chem. Phys.* **130**, 531–535 (2011).
29. Ullah, R. & Dutta, J. Photocatalytic degradation of organic dyes with manganese-doped ZnO nanoparticles. *J. Hazard. Mater.* **156**(1–3), 194–200 (2008).
30. Rajbongshia, B. M. & Samdarshi, S. K. ZnO and Co-ZnO nanorods—Complementary role of oxygen vacancy in photocatalytic activity of under UV and visible radiation flux. *Mater. Sci. Eng. B* **182**, 21–28 (2014).
31. Xiao, Q., Zhang, J., Xiao, C. & Tan, X. Photocatalytic decolorization of methylene blue over $Zn_{1-x}Co_xO$ under visible light irradiation. *Mater. Sci. Eng. B* **142**(2–3), 121–125 (2007).
32. Fu, M. *et al.* Sol–gel preparation and enhanced photocatalytic performance of Cu-doped ZnO nanoparticles. *Appl. Surf. Sci.* **258**(4), 1587–1591 (2011).
33. Kanade, K. G. *et al.* Self-assembled aligned Cu doped ZnO nanoparticles for photocatalytic hydrogen production under visible light irradiation. *Mater. Chem. Phys.* **102**(1), 98–104 (2007).
34. Kyaw, K. K. & Toe, H. Characterization and doping effect of Cu-doped ZnO Films. *J. Mater. Sci. Eng. A* **10**(3–4), 43–52 (2020).
35. Páez, C. A. *et al.* Study of photocatalytic decomposition of hydrogen peroxide over ramsdellite-MnO_2 by O_2-pressure monitoring. *Catal. Commun.* **15**, 132–136 (2011).

36. Casas-Cabanas, M. *et al.* Defect Chemistry and Catalytic Activity of Nanosized Co_3O_4. *Chem. Mater.* **21**(9), 1939–1947 (2009).
37. Li, X., Chen, Ch. & Zhao, J. Mechanism of photodecomposition of H_2O_2 on TiO_2 surfaces under visible light irradiation. *Langmuir* **17**(13), 4118–4122 (2001).
38. Wolski, L., Walkowiak, A. & Ziolek, M. Formation of reactive oxygen species upon interaction of Au/ZnO with H_2O_2 and their activity in methylene blue degradation. *Catal. Today* **333**, 54–62 (2019).
39. Bahsi, Z. & Oral, A. Effect of Mn and Cu doping on the microstructures and optical properties of Sol-Gel derived ZnO thin films. *Opt. Mater.* **29**(6), 672–678 (2007).
40. Widiarti, N., Sae, J.K & Wahyuni, S.: Synthesis CuO-ZnO nanocomposite and its application as an antibacterial agent. *IOP Conf. Ser. Mater. Sci. Eng.* **172**, 012036 (2017).
41. Shohel, M., Miran, M. S., Susan, M. A. B. H. & Mollah, M. Y. A. Calcination temperature-dependent morphology of photocatalytic ZnO nanoparticles prepared by an electrochemical–thermal method. *Res. Chem. Intermed.* **42**, 5281–5297 (2016).
42. Bloh, J. Z., Dillert, R. & Bahnemann, D. W. Transition metal-modified zinc oxides for UV and visible light photocatalysis. *Environ. Sci. Pollut. Res.* **19**(9), 3688–3695 (2012).
43. Ao, D. *et al.* Heterostructured NiO/ZnO nanorod arrays with significantly enhanced H_2S sensing performance. *Nanomaterials* **9**, 2–13 (2019).
44. Panchatcharam, P. Multilayer thin films—versatile applications for materials engineering. chapter: synthesis and characterization of CoO-ZnO-based nanocomposites for gas-sensing applications. https://doi.org/10.5772/intechopen.88760 (2020).
45. Widiarti, N., Sae, J. K. & Wahyuni, S. Synthesis CuO-ZnO nanocomposite and its application as an antibacterial agent. *IOP Conf. Ser. Mater. Sci. Eng.* **172**, 1–12 (2017).
46. Lousada, C. M., Johansson, A. J., Brinck, T. & Jonsson, M. Mechanism of H_2O_2 decomposition on transition metal oxide surfaces. *J. Phys. Chem. C* **116**, 9533–9543 (2012).
47. Salem, I. A. Catalytic decomposition of H_2O_2 over supported ZnO. *Monatshefte für Chemie* **131**, 1139–1150 (2000).
48. Kotrly, S. & Sucha, L. *Handbook of Chemical Equilibria in Analytical Chemistry* **221** (Ellis Horwood, Chichester, 1985).
49. Devi, L. G., Kottam, N., Murthy, B. N. & Kumar, S. G. Enhanced photocatalytic activity of transition metal ions Mn^{2+}, Ni^{2+} and Zn^{2+} doped polycrystalline titania for the degradation of Aniline Blue under UV/solar light. *J. Mol. Catal. A Chem.* **328**, 44–52 (2010).
50. Bundgaard, E. & Krebs, F. C. Low band gap polymers for organic photovoltaics. *Solar Energy Mater. Solar Cells* **91**(11), 954–985 (2007).
51. Hirakawa, T. & Nosaka, Y. Properties of $O_2^{\bullet-}$ and OH• formed in TiO_2 aqueous suspensions by photocatalytic reaction and the influence of H_2O_2 and some ions. *Langmuir* **18**, 3247–3254 (2002).
52. Irie, H., Miura, S., Kamiya, K. & Hashimoto, K. Efficient visible light- sensitive photocatalysts: grafting Cu (II) ions onto TiO_2 and WO_3 photocatalysts. *Chem. Phys. Lett.* **457**, 202–205 (2008).
53. Cho, J. M. *et al.* Effects of ultraviolet–ozone treatment on organic-stabilized ZnO nanoparticle-based electron transporting layers in inverted polymer solar cells. *Organ. Electron.* **15**, 1942–1950 (2014).
54. Pati, S. S. *et al.* Facile approach to suppress γ-Fe_2O_3 to α-Fe_2O_3 phase transition beyond 600 °C in Fe_3O_4 nanoparticles. *Mater. Res. Exp.* **2**(4), 045003 (2015).

Acknowledgements

The director of this research, Beto Páez, passed away this July 12th. Beto was a researcher, full of ideas, super enthusiastic, super nice ... and in love. This paper is dedicated to the memory of Dr. Carlos Alberto (Beto) Páez (July 1974-July 2020).

Author contributions

A.E.R. and C.A.P. conceived and designed the experiments and analyzed the data. M.M., J.E.R. and J.A.C. characterized the optical properties of the samples. A.E.R. in collaboration with L.L.L. characterized the structure os samples by TEM, XRD, XRF. The manuscript was written by A.E.R. and C.A.P. with input from J.A.C. and B.H.

Funding

A. Ramírez acknowledges the financial support obtained from CNPq/CLAF (Fellowship for Postdoctoral Young Research Program), Belgian F.R.S.-FNRS and Universidad del Cauca (VRI ID-4737). C.A. Páez and B. Heinrichs thank the Belgian Fonds de la Recherche Fondamentale Collective (F.R.F.C), the Ministère de la Région Wallonne. JAHC thanks the Brazilian agencies CNPq (301455/2017-1, 443652/2018-0) and FAPDF (00193.0000151/2019-20) for the financial support.

Competing interests

The authors declare no competing interests.

Additional information

Correspondence and requests for materials should be addressed to A.E.R.

Reprints and permissions information is available at www.nature.com/reprints.

Publisher's note Springer Nature remains neutral with regard to jurisdictional claims in published maps and institutional affiliations.